ELSEVIER

Catalysis Today 50 (1999) 109–116

CATALYSIS TODAY

Simulation of a solid oxide fuel cell for oxidative coupling of methane

Guo Xui-Mei, Kus Hidajat*, Chi-Bun Ching

Department of Chemical and Environmental Engineering, National University of Singapore, Singapore 119260, Singapore

Abstract

Oxidative coupling of methane in a solid oxide fuel cell with 1 wt% Sr/La_2O_3–Bi_2O_3–Ag–YSZ (yttria stabilized zirconia) membrane was studied by the two mathematical models based on well mixed flow (CSTM) or plug flow (PFM). The model predictions were in good agreement with the experimental results. The performance of the solid oxide fuel cell was evaluated by investigating the effect of reaction conditions and the degree of back mixing. © 1999 Elsevier Science B.V. All rights reserved.

Keywords: Solid oxide fuel cell; Oxidative coupling; Yttria stabilized zirconia (YSZ)

1. Introduction

More and more attention has been focused on atmospheric pollution and greenhouse warming in the recent years due to the increase in global warming rate. CO_2 is considered to be responsible for about half of the global warming rate. Solid oxide fuel cells have the advantages of high efficiency, low pollution, simplified system, high power density and so on which make them very attractive for utility and industrial applications. If the electrical energy and useful chemicals can be cogenerated in a solid oxide fuel cell, it will be much more attractive not only from an energy conversion, but also from an environmental standpoint. The oxidative coupling of methane to ethane and ethene shows great potential as a novel use of natural gas. It is in this direction that considerable efforts have been made to attain active and selective catalysts for the reaction. C_2 yield up to the order of 25% has been reported [1]. The oxidation of methane to ethane and ethylene in solid oxide fuel cells has opened up a new way for the utilization of natural gas. In the solid oxide fuel cell, as shown in Fig. 1, an oxygen ion conducting membrane separates an oxygen source from the fuel. The oxygen is reduced to oxygen ion on the cathode and transferred through the membrane to the anode, on which the active oxygen species react with methane to form ethane and ethylene. During the reaction, electrons discharged in the anode return to the cathode via an external circuit. The driving force for the operation is the chemical potential gradient of oxygen across the membrane.

Besides the above advantages, in the solid oxide fuel cell, oxygen can be separated from air, thus the separation process can be simplified and the amount of the gases out of the product side of reactors can be decreased. The reactants are separated from the oxygen source by the membrane, leading to a diminishing of the explosion hazards. Cogeneration of electrical

*Corresponding author. Tel.: +65-8742191; fax: +65-7791936; e-mail: chedidak@nus.edu.sg

0920-5861/99/$ – see front matter
PII: S0920-5861(98)00467-2

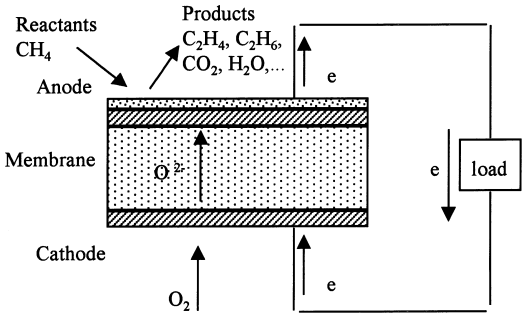

Fig. 1. A schematic diagram of a solid oxide fuel cell.

energy and useful chemicals such as NO, HCN, C_2 hydrocarbons and so on in the solid oxide fuel cells has been studied [2,3]. A review has been given by Eng and Stoukides [4]. However, most of the studies have been focused on the experiments. Analysis and simulation are necessary to investigate the properties and performance of the solid oxide fuel cell and provide the efficient design and operation.

In this paper, two mathematical models are presented to describe the behaviour of the solid oxide fuel cells. The oxidative coupling of methane catalysed by 1 wt% Sr/La_2O_3–Bi_2O_3–Ag–YSZ is used as a model reaction.

$$CH_4 + O_2 \rightarrow C_2(C_2H_4, C_2H_6) + H_2O$$

Methane and C_2 hydrocarbons can react with oxygen further to form carbon dioxide and water, which is thermodynamically favoured over the above reactions.

$$CH_4 + O_2 \rightarrow CO_2 + H_2O$$

$$C_2(C_2H_4, C_2H_6) + O_2 \rightarrow CO_2 + H_2O$$

2. Experimental set-up

An experimental apparatus was set up to examine the cogeneration of ethane and ethylene and electrical energy in the solid oxide fuel cell, as shown in Fig. 2. The fuel cell was of tube–shell type. The cell was constructed from a quartz tube of 22 mm ID enclosed by a solid oxide membrane tube of 11 mm OD, 1 mm thickness and 50 mm coating length. The solid oxide membrane consisted of three layers: 8 mol% yttria stabilized zirconia (YSZ) layer, Ag electrode layer and 1 wt% Sr/La_2O_3–Bi_2O_3 catalyst layer. The preparation

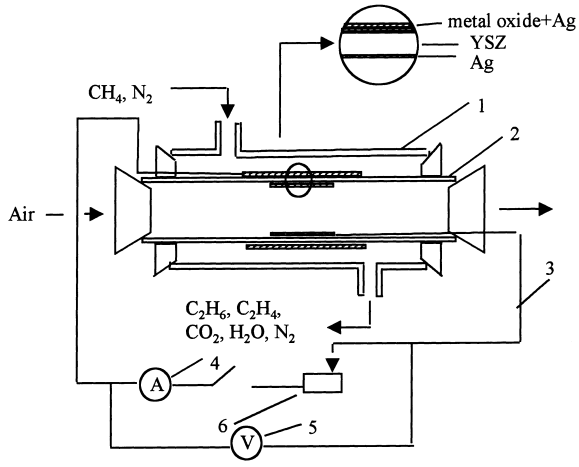

Fig. 2. The configuration of solid oxide fuel cell: (1) quartz tube; (2) YSZ tube; (3) Ag wire; (4) multimeter used as galvanometer; (5) multimeter used as voltmeter; (6) resistance box.

method of the membrane was described in our previous study [8]. The reaction gas, CH_4 diluted in N_2, was fed to the annular space between the quartz and the membrane tube at a total flow rate of 1.67 ml s^{-1}. Air was fed co-currently to the tube side of the fuel cell at the flow rate of 3.34 ml s^{-1}. The fuel cell was placed in a furnace controlled within 1–2 K with a EUROTHERM808 temperature controller. The voltage and the current were measured with two HP34401A multimeters, respectively. N72 resistance box was used to change the load. Ag wire was attached to the membrane tube to carry the current to the external circuit. Analysis of reactants and products was performed using an on-line gas chromatography with two columns packed with Porapak Q and molecular sieve 5 A. All experiments were performed at atmospheric pressure.

3. Modelling

A schematic diagram of the solid oxide fuel cell with shell-tube type is shown in Fig. 3. A single or multiple reactions may take place at the membrane, and the general reaction rate of component j is represented by

$$R_j = \sum_{i=1}^{m} \gamma_{ij} r_i \quad (j = 1, 2, \ldots, n). \tag{1}$$

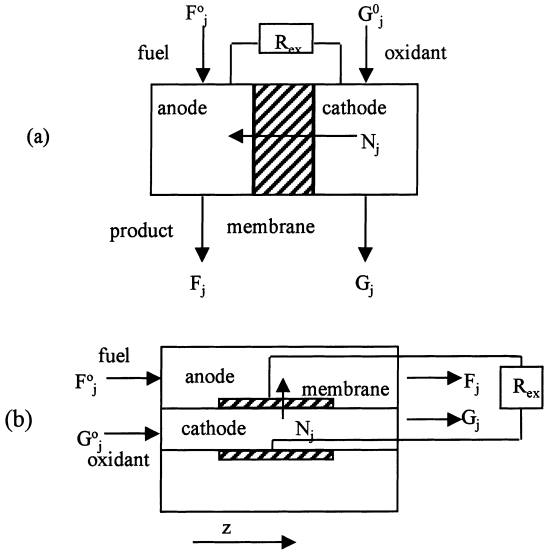

Fig. 3. Schematic illustration of CSTM and PFM: (a) CSTM; (b) PFM.

The continuously stirred tank model (CSTM) and the plug flow model (PFM) are used to describe the behaviour of the solid oxide fuel cells. The two models are based on the following assumptions: well mixed anodic and cathodic chambers for CSTM and plug flow in anodic and cathodic chambers for PFM, constant pressure, isothermal, steady-state operation, negligible mass transfer resistance and ideal gas behaviour.

Based on these assumptions, the CSTM equations for the well-mixed flow in both shellside and tubeside of the solid oxide fuel cell are derived by taking the material balance for each component in the shellside and the tubeside.

In the shellside:

$$F_j^0 - F_j + N_j - S_r R_j = 0 \quad (j = 1, 2, \ldots, n). \tag{2}$$

In the tubeside:

$$G_j^0 - G_j - N_j = 0 \quad (j = 1, 2, \ldots, n). \tag{3}$$

Due to the fact that the oxygen ion solid electrolytes such as YSZ, are a pure ionic conductor, it can be considered that other components except oxygen cannot permeate through the membrane. According to Faraday's law, the oxygen permeation flux can be written as

$$\mathrm{N}_{\mathrm{O}_2} = \frac{I}{4f}, \qquad N_j = 0 \quad (j \neq \mathrm{O}_2,\ j = 1, 2, \ldots, n). \tag{4}$$

The cell current appearing in the above equation is related to cell voltage by

$$E = IR_{\mathrm{ex}}, \tag{5}$$

in which R_{ex} is the external resistance.

When the external load is finite and the cell produces power, the voltage drops below the reversible voltage due to slow reaction or mass transfer. The cell voltage can be calculated as follows:

$$E = E_{\mathrm{rev}} - (\phi_{\mathrm{o}} + \phi_{\mathrm{act}} + \phi_{\mathrm{conc}}), \tag{6}$$

where E_{rev} is reversible cell voltage and can be given as

$$E_{\mathrm{rev}} = \frac{n(-\Delta G)}{4f}. \tag{7}$$

ϕ_{o} is the ohmic overpotential, which is the voltage drop across the electrolyte–electrode assembly and can be written as

$$\phi_{\mathrm{o}} = (R_{\mathrm{el}} + R_i)I, \tag{8}$$

where R_{el} includes electrolyte–electrode contact losses, ohmic losses across the porous electrode and electrode current collector losses. R_i is the electrolyte resistance, which can be written as

$$R_i = A \exp(E^*/RT) \frac{h}{A_{\mathrm{el}}}, \tag{9}$$

where h is the electrolyte thickness, A_{el} the superficial electrode area, A the electrolyte resistivity perexponential factor and E^* is the activation energy for O^{2-} conduction in solid electrolyte.

ϕ_{act} is the activation overpotential, which can be calculated by Butler–Volmer equation [5]:

$$\frac{I}{I_0} = \exp(\alpha_{\mathrm{a}} F \phi_{\mathrm{act}}/RT) - \exp(\alpha_{\mathrm{c}} F \phi_{\mathrm{act}}/RT), \tag{10}$$

where ϕ_{act} is an implicit function of I, T and other parameters.

Using the high field approximation (ϕ_{act}>100 mV), ϕ_{act} can be written as

$$\phi_{\mathrm{act}} = \frac{RT}{\alpha_{\mathrm{a}} F} \ln \frac{I}{I_{0,\mathrm{a}}} + \frac{RT}{\alpha_{\mathrm{c}} F} \ln \frac{I}{I_{0,\mathrm{c}}}. \tag{11}$$

Using the low field approximation (ϕ_{act}<10 mV), ϕ_{act} can be written as

$$\phi_{act} = \frac{RT}{(\alpha_a + \alpha_c)F}\frac{I}{I_0}. \quad (12)$$

A numerical technique can be used to evaluate by the iteration between Eqs. (11) and (12) for the 10 mV<ϕ_{act}<100 mV.

ϕ_{conc} is concentration overpotential and can be given as

$$\phi_{conc} = \frac{-RT}{nF}\left(\ln\left(1 - \frac{I}{I_{L,c}}\right) + \ln\left(1 - \frac{I}{I_{L,a}}\right)\right), \quad (13)$$

where $I_{L,a}$ and $I_{L,c}$ are the limiting anodic and cathodic currents.

The PFM equations for the plug flow in both shellside and tubeside of the solid oxide fuel cell (as shown in Fig. 2) are as follows:

In the shellside:

$$\frac{dF_j}{dz} + \frac{N_j}{L} - \frac{S_r R_j}{L} = 0 \quad (j = 1, 2, \ldots, n). \quad (14)$$

In the tubeside:

$$\frac{dG_j}{dz} - \frac{N_j}{L} = 0 \quad (j = 1, 2, \ldots, n). \quad (15)$$

The boundary conditions are:

at z=0, in the shellside

$$F_j = F_j^0 \quad (j = 1, 2, \ldots, n), \quad (16)$$

in the tubeside

$$G_j = G_j^0 \quad (j = 1, 2, \ldots, n). \quad (17)$$

The rest of the equations of PFM is the same as that of CSTM.

The reaction rate expressions for oxidative coupling of methane were derived according to the mechanism proposed elsewhere [6]. The detailed kinetic investigations were performed to calculate the values of the pertinent kinetic constants. The following expressions of ethane, ethylene and carbon dioxide formation rates were obtained:

(1) Absence of gas phase oxygen in the shellside:

$$r_{C_2H_6} = \frac{(k_1 y_{CH_4} - k_3 y_{C_2H_6}) J_{O_2}}{k_1 y_{CH_4} + k_3 y_{C_2H_6}} - \frac{k_6 K_4 y_{C_2H_6} J_{O_2}}{k_1 y_{CH_4} + k_3 y_{C_2H_6} + K_4 J_{O_2}} - k_5 y_{C_2H_6}, \quad (18)$$

$$r_{C_2H_4} = \frac{k_3 y_{C_2H_6} J_{O_2}}{k_1 y_{CH_4} + k_3 y_{C_2H_6}} - \frac{k_7 K_4 y_{C_2H_4} J_{O_2}}{k_1 y_{CH_4} + k_3 y_{C_2H_6} + K_4 J_{O2}} + k_5 y_{C_2H_6}, \quad (19)$$

$$r_{CO_2} = \frac{(k_6 y_{C_2H_6} + k_7 y_{C_2H_4}) K_4 J_{O_2}}{k_1 y_{CH_4} + k_3 y_{C_2H_6} + K_4 J_{O_2}}. \quad (20)$$

(2) Presence of gas phase oxygen in the shellside:

$$r_{C_2H_4} = \frac{(k_1 y_{CH_4} - k_3 y_{C_2H_6})\left[J_{O_2}\left(\sqrt{K_8} + \sqrt{y_{O_2}}\right) + k_{-4}\sqrt{y_{O_2}}\right]}{\left(\sqrt{K_8} + \sqrt{y_{O_2}}\right)(k_1 y_{CH_4} + k_3 y_{C_2H_6}) + k_4\sqrt{K_8}} - \frac{k_6 y_{C_2H_6}\sqrt{y_{O_2}}}{\left(\sqrt{K_8} + \sqrt{y_{O_2}}\right)} - k_5 y_{C_2H_6}, \quad (21)$$

$$r_{C_2H_4} = \frac{k_3 y_{C_2H_6}\left[J_{O_2}\left(\sqrt{K_8} + \sqrt{y_{O_2}}\right) + k_{-4}\sqrt{y_{O_2}}\right]}{\left(\sqrt{K_8} + \sqrt{y_{O_2}}\right)(k_1 y_{CH_4} + k_3 y_{C_2H_6}) + k_4\sqrt{K_8}} - \frac{k_7 y_{C_2H_4}\sqrt{y_{O_2}}}{\left(\sqrt{K_8} + \sqrt{y_{O_2}}\right)} + k_5 y_{C_2H_6}, \quad (22)$$

$$r_{CO_2} = \frac{(k_6 y_{C_2H_6} + k_7 y_{C_2H_4})\sqrt{y_{O_2}}}{\left(\sqrt{K_8} + \sqrt{y_{O_2}}\right)}. \quad (23)$$

By fitting the experimental data, the values of kinetic parameters in Eqs. (18)–(23) are given below in Table 1.

Table 1
Values of kinetic parameters

Parameter	Arrhenius constants	
	A	E^*
k_1	0.7176×10^{-3}	0.6319×10^{2}
k_3	0.1415×10^{3}	0.1074×10^{3}
k_4	0.3473×10^{2}	0.9349×10^{2}
k_{-4}	0.1845×10^{3}	0.8994×10^{2}
k_5	0.9760×10^{2}	0.1012×10^{3}
k_6	0.9420×10^{2}	0.9284×10^{2}
k_7	0.9609×10^{2}	0.9069×10^{2}
K_4	0.1074×10	0.4836×10^{3}
K_8	0.2607×10^{-2}	0.1196×10^{3}

CH_4 conversion and C_2 selectivity were calculated by

$$X_{CH_4} = (F^0_{CH_4} - F_{CH_4})/F^0_{CH_4}, \quad (24)$$

$$S_{C_2} = 2(F_{C_2H_4} + F_{C_2H_6})/(F^0_{CH_4} - F_{CH_4}). \quad (25)$$

4. Results and discussion

The set of CSTM model equations was non-linear. The modified Newton–Raphson method was employed to solve them numerically. The set of PTM model equations was ordinary differential–algebraic equations, which was solved by the Petzold–Gear's backward differentiation formulas (BDF) method after the equations were transformed.

4.1. Model simplification

Ohmic overpotential was the predominant source of polarization in most applications of solid oxide fuel cells. Concentration overpotential was due to slow mass transfer of reactants and/or products involved in the charge-transfer reaction. Contrary to aqueous electrochemistry, where concentration overpotential was frequently important due to low reactant and/or product diffusivities in the aqueous phase, in solid oxide fuel cells mass transfer in the gas phase was fast. Consequently, concentration overpotential was negligible in solid oxide fuel cells. Activation overpotential was caused by slow reaction and electron transfer at electrode–electrolyte interface, and could be decreased by using a good electrocatalyst with a high exchange current. Activation overpotential was frequently negligible in solid oxide fuel cells compared with ohmic overpotential [7]. However, for the reaction of oxide coupling of methane, the activation overpotential could not be neglected because no satisfactory electrocatalyst had been found.

4.2. Comparison of simulated results and experimental results

As shown in Figs. 4 and 5, the results of the simulation and the experiment were compared with investigating the relationships among C_2 selectivity, CH_4 conversion, power output and generated current. The feed composition, flow rate and temperature were kept relatively constant. It was noted that both of the

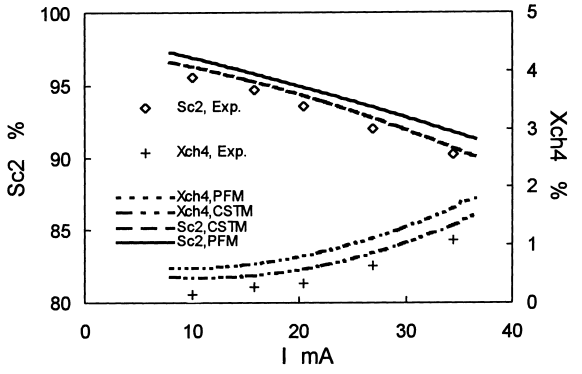

Fig. 4. C_2 selectivity and CH_4 conversion versus current. T=1003.15 K; anode: F_t=3.41×10^{-5} mol s^{-1}; P_{CH_4} = 20.3 kPa; cathode: Q_t=1.705×10^{-4} mol s^{-1}; P_{O_2} = 21.3 kPa.

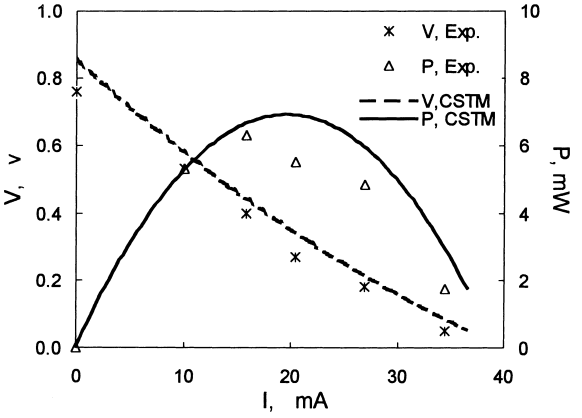

Fig. 5. Voltage–current and power–current (reaction conditions are the same as those of Fig. 4).

simulated results of the models were slightly higher than the experimental results. This might be due to the negligence of interfacial mass transfer resistance between the gas phase and the surface of membrane and the internal mass transfer resistance in the membrane when the simulation was carried out. In addition, it could be also found that the simulated results of CSTM were much closer to the experimental data. Under the flow rates employed in this study, though the solid oxide fuel cell was in the tubular shape, the length-to-diameter ratio was relatively small in the present experimental set-up, leading to the behaviour in the solid oxide fuel cell resembling in a continuous flow stirred tank reactor (CSTR). However, the tendency of simulated results and experimental results

was consistent and the agreement could be considered to be satisfactory according to the goal of the study.

4.3. *Effect of operating conditions on the performance of the solid oxide fuel cell*

In this study, the performance of the solid oxide fuel cell was evaluated by examining the influence of operating conditions such as external load, temperature, feed composition on C_2 selectivity, CH_4 conversion and current generated. The relationships among C_2 selectivity, CH_4 conversion and the current generated were shown in Fig. 4. CH_4 conversion increased and C_2 selectivity decreased with increasing current generated in the solid oxide fuel cell. It indicated that an increase in C_2 selectivity was accompanied with a drop in current and CH_4 conversion in the solid oxide fuel cell.

The current–voltage and current–power plots at constant temperature, feed composition, total flow rate is also given in Fig. 5. The voltage obtained under open circuit reached 0.85 V and decreased quasi-linearly with increasing current. It demonstrated that ohmic overpotential was the dominant source of polarization at the temperature range. Therefore, it verified that the above model simplifications were reasonable. The electrical power output increased with current until it reached a point as indicated above, after which it decreases. At that point there was an optimal load so that the power output became maximum.

Fig. 6 showed the effect of temperature on C_2 selectivity and CH_4 conversion at constant feed composition and total flow rate. It was seen that C_2 selectivity initially increased with a rise in temperature and then started decreasing. C_2 selectivity showed maximum at about 1033 K. CH_4 conversion showed an increase with increasing temperature. Fig. 7 showed the effect of temperature on the current generated. It could be seen that the current generated increased with temperature. This was due to the increased ionic conductivity of the YSZ at the higher temperatures.

The dependency of the ethylene-to-ethane ratio on temperature is given in Fig. 8. It was noted that the ratio increased with a rise in temperature. The reaction network for the reaction was generally accepted that ethylene was formed from ethane [9]. With the increase in temperature, the oxidative dehydrogena-

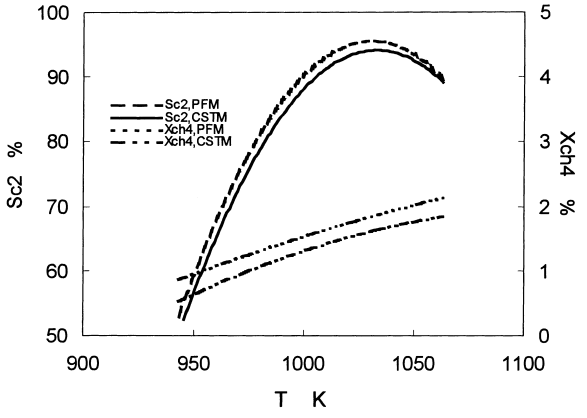

Fig. 6. C_2 selectivity and CH_4 conversion as a function of temperature. R_{ex}=0.1 Ω; anode: F_t=3.41×10^{-5} mol s^{-1}; P_{CH_4} = 20.3 kPa; cathode: Q_t=1.705×10^{-4} mol s^{-1}; P_{O_2} = 21.3 kPa.

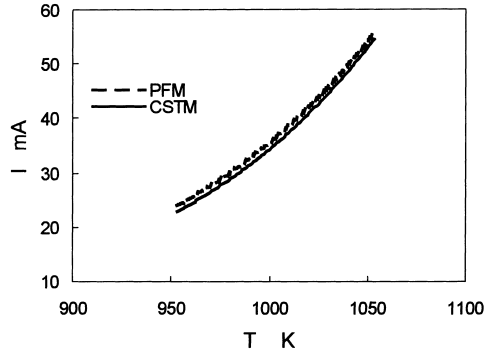

Fig. 7. Current as a function of temperature (reaction conditions are the same as those of Fig. 6).

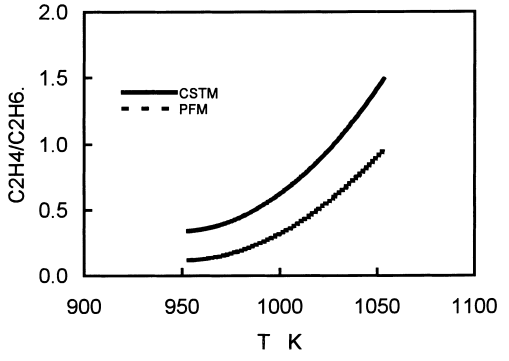

Fig. 8. C_2H_4/C_2H_6 as a function of temperature (reaction conditions are the same as those of Fig. 6).

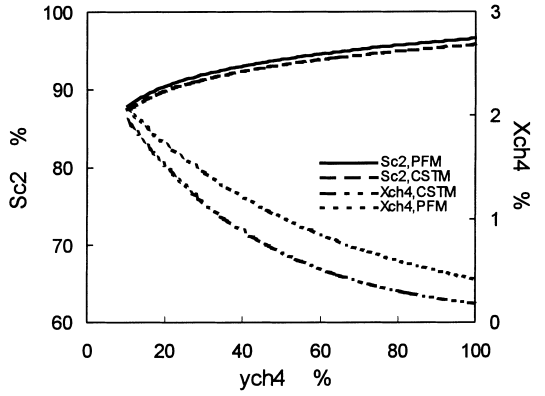

Fig. 9. C_2 selectivity and CH_4 conversion as a function of feed composition. T=1003.15 K; R_{ex}=0.1 Ω; anode: F_t=3.41×10^{-5} mol s^{-1}; cathode: Q_t=1.705×10^{-4} mol s^{-1}; P_{O_2} = 21.3 kPa.

tion of ethane was enhanced, resulting in the increase in the ratio of ethylene to ethane.

Fig. 9 showed the C_2 selectivity and CH_4 conversion as a function of feed composition. CH_4 conversion decreased with a rise in feed CH_4 concentration. C_2 selectivity increased obviously when methane mole fraction was low. When methane mole fraction was greater than about 60%, C_2 selectivity increased slightly.

4.4. Comparison of the predictions of the two models

Figs. 4–9 show that there were differences between the predictions of the two models. For PFM, all CH_4 conversion, C_2 selectivity and current generated were higher than these for CSTM, but the ratio of ethylene to ethane was lower. It was probably caused by the fact that the C_2 products were relatively unstable and that the back-mixing of the C_2 products led to transporting the products to the regions where the oxygen concentration was relatively high. Thus the C_2 products were oxidized further and a low C_2 selectivity was obtained.

5. Conclusions

Two mathematical models were developed to describe the behaviour of solid oxide fuel cells. The agreement between the simulated and experimental results was satisfactory. Using the two models, the effect of the various operating parameters on the performance of oxidative coupling of methane was investigated. The degree of back-mixing in the solid oxide fuel cell influenced the CH_4 conversion, C_2 selectivity, current generated and the ratio of ethylene to ethane. In the study, the experimental results are close to the simulated results of CSTM.

6. Nomenclature

A	electrolyte resistivity preexponential factor (Ω)
A_{el}	superficial electrode surface area (m^2)
E	cell voltage (V)
E^*	activation energy (J mol^{-1})
F_j	mole flow rate of component j in the shellside (mol s^{-1})
f	Faraday constant
G	mole flow rate of component j in the tubeside (mol s^{-1})
h	electrolyte thickness (m)
I	current (A)
$I_{0,a}$	anodic exchange current (A)
$I_{0,c}$	cathodic exchange current (A)
$I_{L,a}$	limiting anodic current (A)
$I_{L,c}$	limiting cathodic current (A)
J	oxygen flux (mol s^{-1})
K	equilibrium constant
k	reaction rate constant (mol m^{-2} s^{-1})
L	reactor length (m)
m	number of reaction
N	permeation flux (mol s^{-1})
n	number of component
P	power (W)
P_i	i component partial pressure (Pa)
R	gas constant
R_{el}	electrode resistance (Ω)
R_{ex}	external load (Ω)
R_i	electrolyte resistance (Ω)
R_j	general reaction rate of component j (mol m^{-2} s^{-1})
r	reaction rate (mol m^{-2} s^{-1})
S_{C_2}	C_2 selectivity (%)
S_r	effective reaction area (m^2)
T	temperature (K)
X_{CH_4}	CH_4 conversion (%)
y	mole fraction (%)
Z	longitudinal distance (m)

Greek symbols

α_a, α_c	transfer coefficient for anodic and cathodic overpotential
γ	stoichiometric coefficient
ΔG	Gibbs free energy change
ϕ_{act}	activation overpotential (V)
ϕ_{conc}	concentration overpotential (V)
ϕ_o	ohmic overpotential (V)

Superscript

0	feed condition

Subscript

t	total
i	reaction *i*
j	component *j*
rev	reversible condition

References

[1] Y. Amenomiya et al., Catal. Rev.-Sci. Eng. 32(3) (1990) 163.
[2] K. Otsuka, K. Suga, I. Yamanaka, Catal. Today 6 (1990) 587.
[3] N. Kiratzis, M. Stoukides, J. Electrochem. Soc. 134(8) (1987) 1925.
[4] D. Eng, M. Stoukides, Catal. Rev.-Sci. Eng. 33 (1991) 375.
[5] A.J. Bard, L.R. Faulkner, Electrochemical Methods: Fundamentals and Applications, Wiley, New York, 1980.
[6] G. Xiu-Mei, C. Hong-Fang, J. Chem. Ind. Eng. (China) 46(3) (1995) 310.
[7] C.G. Vayenas, S. Bebelis, I.V. Yentekakis, H.-G. Lintz, Catal. Today 11(3) (1992) 303.
[8] G. Xiu-Mei, K. Hidajat, C.-B. Ching, Ind. Eng. Chem. Res. 36 (1997) 3576.
[9] J.S. Lee, S.T. Oyama, Catal. Rev.-Sci. Eng. 30(2) (1988) 249.